Front. Earth Sci. 2018, 12(3): 457–467
https://doi.org/10.1007/s11707-018-0728-6

RESEARCH ARTICLE

Assimilation of atmospheric infrared sounder radiances with WRF-GSI for improving typhoon forecast

Yan-An LIU[1,2,3,4,5], Zhibin SUN (✉)[3,5], Maosi CHEN[5], Hung-Lung Allen HUANG[3,6], Wei GAO (✉)[3,4,5]

1 Key Laboratory of Geographic Information Science (Ministry of Education), East China Normal University, Shanghai 200241, China
2 School of Geographic Sciences, East China Normal University, Shanghai 200241, China
3 ECNU-CSU Joint Research Institute for New Energy and the Environment, East China Normal University, Shanghai 200062, China
4 Joint Laboratory for Environmental Remote Sensing and Data Assimilation, East China Normal University, Shanghai 200241, China
5 Natural Resource Ecology Laboratory, Colorado State University, Fort Collins, CO 80523, United States
6 Cooperative Institute for Meteorological Satellite Studies, University of Wisconsin-Madison, Madison, WI 53706, United States

Abstract The Atmospheric Infrared Sounder (AIRS) can provide the profile information on atmospheric temperature and humidity in high vertical resolution. The assimilation of its radiances has been proven to improve the Numerical Weather Prediction (NWP) in global models. In this study, regional assimilation of AIRS radiances was carried out in a community assimilation system, using Gridpoint Statistical Interpolation (GSI) coupled with the Weather Research and Forecasting (WRF) model. The AIRS channel selection, quality control, and radiances bias correction were examined and illustrated for optimized assimilation. The bias correction scheme in the regional model showed that corrections on most of the channels produce satisfactory results except for several land surface channels. The assimilation and forecast experiments were carried out for three typhoon cases (Saola, Damrey, and Haikui in 2012) with and without including AIRS radiances. Results show that the assimilation of AIRS radiances into the WRF/GSI model improves both the typhoon track and intensity in a 72-hour forecast.

Keywords AIRS, WRF/GSI model, radiance assimilation, typhoon forecast

1 Introduction

With the gradual improvement on Numerical Weather Prediction (NWP) models, the accuracy of the initial field of the model has become a key factor to the numerical forecasting (Bauer et al., 2015). Meteorological satellite observation data can provide continuous and consistent atmospheric state information, which can not only fill gaps in areas with severe lack of atmospheric exploration data (e.g., oceans, mountains, and deserts), but also meet the space-time density requirements of conventional observational data on small and medium-scale weather (Klaes et al., 2007; Goldberg et al., 2013). Therefore, how to fuse different types of satellite observation data, conventional observation data and other types of observation data into a more accurate and reliable initial field data has become one of the core components in NWP research.

As the most important observation source for improving global numerical weather prediction, hyperspectral infrared sounding measurements can provide atmospheric structure information with high temporal and spatial resolution (Menzel et al., 2018). Different from conventional observations, the satellite observation data does not act as a model variable, and has nonlinear relationships with the temperature, humidity, and other variables in the model. Satellite radiances can be directly assimilated into the model based on radiative transfer models, so as to avoid the complex observational error descriptions during the inversion assimilation.

The Atmospheric Infrared Sounder (AIRS) is relatively mature and stable in global model assimilation applications due to its early launch. It can provide a complete reference for the application of hyperspectral infrared data in regional models. Many researchers have assimilated the hyperspectral infrared data into global and regional models with great success.

In early applications of AIRS assimilation, the retrieved

Received April 16, 2018; accepted July 19, 2018

E-mails: Zhibin.Sun@colostate.edu (Zhibin SUN), wgao@geo.ecnu.edu.cn (Wei GAO)

temperature and humidity profile assimilation were dominant. Li and Liu (2009) assimilated the AIRS Field of View (FOV) inversion profile to show the improvement of hurricane path and intensity prediction. Zhou et al. (2010) assimilated the temperature profiles retrieved from AIRS in cloudy conditions in a global model to improve the tropical cyclone precipitation forecast. Pu and Zhang (2010) used bias corrected AIRS profiles to improve significantly the simulation and forecast of tropical cyclones. Miyoshi and Kunii (2012) assimilated the AIRS inversion profile product into the WRF Kalman filter system, improving the regional numerical model forecast. Zheng et al. (2015) assimilated AIRS profile data to improve the hurricane track forecasting.

With the development of radiative transmission modes and assimilation technologies, the direct assimilation of radiances has dominated the leading technologies in various operational Numerical Weather Prediction centers, such as the National Centers for Environmental Prediction (NCEP) in the United States and European Centre for Medium-Range Weather Forecasts (ECMWF) in Europe (Eyre et al., 1993). ECMWF started the operationalization of AIRS radiation data assimilation in 2003 (McNally et al., 2006). Le Marshall et al. (2006) assimilated AIRS radiation into the National Centers for Environmental Prediction (NCEP) Global Forecasting System (GFS), improving the simulations of anomalies in the 500 hPa geopotential height field in the southern hemisphere.

With the growing attention to the meso-scale severe weather simulation and forecast, more studies have focused on the application of hyperspectral data in the regional model with high resolution. Carrier et al. (2007, 2008) assimilated AIRS radiance data into mesoscale models with improvements in data quality control, relative sensitivities, and model forecasting. McCarty et al. (2009) proved that AIRS radiance assimilation could improve the forecasting ability of 0–48 hours in the North American Mesoscale (NAM) model. Xu et al. (2013) attempted to assimilate IASI radiation data into the WRFDA (Weather Research and Forecasting Data Assimilation System) to improve the prediction of tropical cyclones. Lim et al. (2014) assimilated AIRS clear-sky radiation data into regional models and assessed its impact on precipitation. Regional satellite data assimilation poses more challenges than global data assimilation due to the spatial and temporal constraints. The limited data coverage has a great influence on the bias correction methods used in most data assimilation systems (Liu et al., 2018). At the same time, compared with the assimilation of microwave radiances with limited channels, the detailed impact analysis of AIRS radiances assimilation with many channels in the regional model is rare.

In this paper, our main objective is to analyze the assimilation diagnosis of hyperspectral infrared radiation data in the regional model, and its influence on typhoon forecasts, which improves our understanding the added value of AIRS data. In previous hyperspectral infrared radiances assimilation articles, there was seldom any bias correction diagnosis for all channels, or analysis of the relationship between incremental analysis and typhoon track and intensity improvement. This paper will focus on the AIRS channel selection and bias correction diagnosis based on WRF and Gridpoint Statistical Interpolation (GSI) coupled model, analyzing its impact on the typhoon track and intensity forecast. This paper is organized as follows. Section 2 describes the AIRS satellite observations. In Section 3 is a simple description of WRF forecast model and GSI assimilation system. In section 4, the channels selection, quality control, bias correction, and the increment analysis are described during the AIRS radiances assimilation. Section 5 assesses the impact on typhoon track and intensity forecast with and without assimilating AIRS radiances data. Section 6 provides the research conclusions.

2 AIRS observations

AIRS was launched on Earth Observation System (EOS) Aqua in May 2002, together with AMSU-A (Advanced Microwave Sounding Unit) and HSB (Humidity Sounder for Brazil). These three components form an infrared and microwave atmospheric sounding system. AIRS is the first generation of high spectral resolution infrared atmospheric detection instrument, with 2378 channels with a scanning width of 1650 km and a sub-satellite point resolution of 13.5 km. Using infrared grating spectroscopy technology, it provides spectral coverage in the 3.74–4.61 μm, 6.20–8.22 μm, and 8.8–15.4 μm (Aumann et al., 2003). Its absolute radiation measurement accuracy is better than 0.2 K. Under the clear condition, the temperature inversion accuracy/vertical resolution is 1 K/1 km, and humidity inversion accuracy/vertical resolution is about 15%/2 km. The spectral coverage of AIRS mainly includes 15 μm CO_2 longwave absorption band, 11 μm atmospheric window, 6.7 μm H_2O absorption band, 4.3 μm CO_2 shortwave absorption band, and O_3, CH_4, N_2O, CO, and SO_2 absorption bands. The strong CO_2 absorption bands are used to detect atmospheric temperature; H_2O absorption bands are used to detect atmospheric humidity and cloud characteristics; and other gas absorption bands are used to detect trace gases (Chahine et al., 2006). AIRS data covers the globe twice per day, enabling continuous observation of atmospheric temperature, humidity profile, and other information. An example of the AIRS observation coverages at the four assimilation windows of 00, 06, 12, 18 UTC is shown in Fig. 1, which also indicates the difference of assimilation observations for the regional model when compared with the global model.

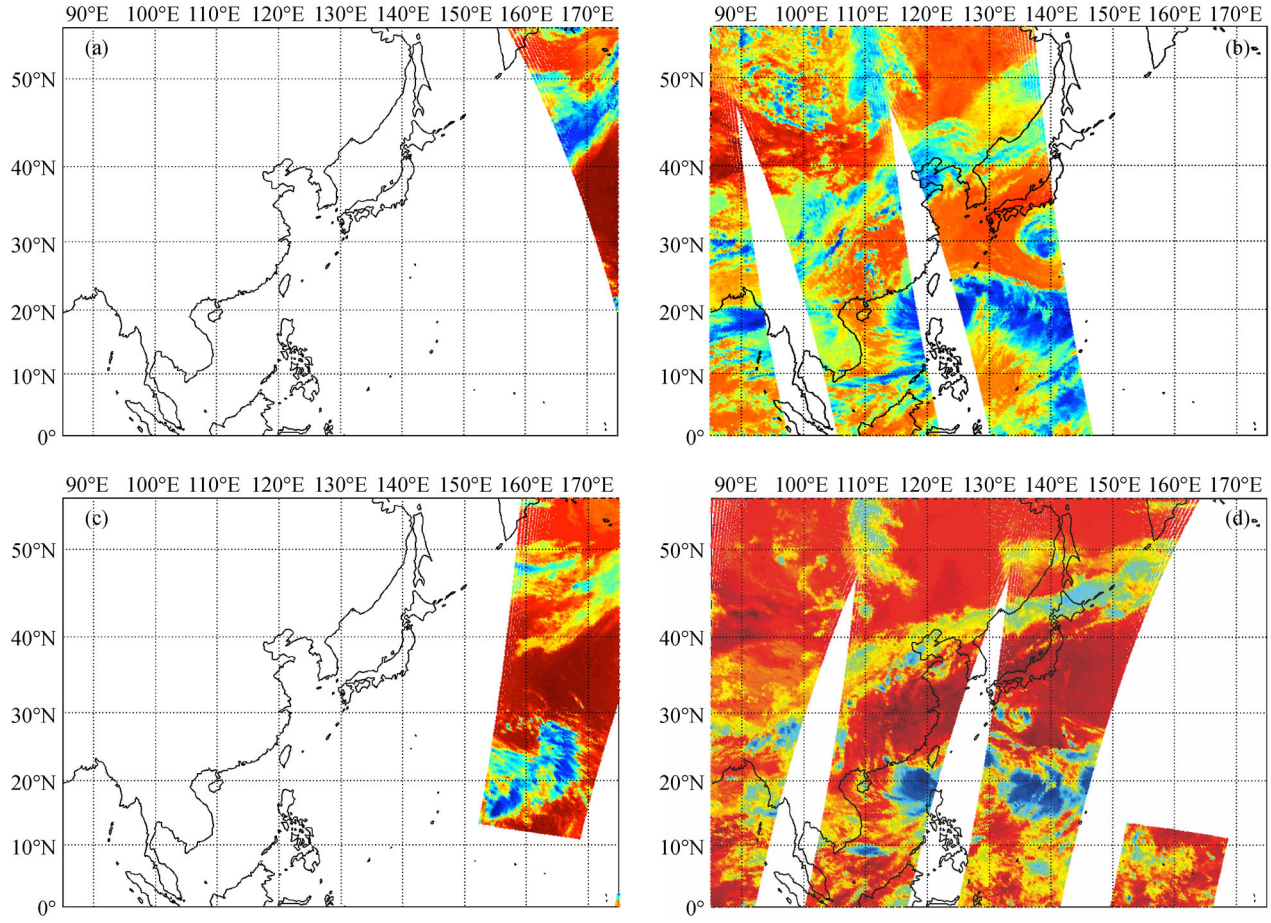

Fig. 1 AIRS data coverage at different assimilation cycles for various analysis times (around±3 h) on 31 July, 2012. (a) 00 UTC; (b) 06 UTC; (c) 12 UTC; (d) 18 UTC.

3 Model description and experiment design

3.1 WRF forecast model

WRF-ARW (V3.5) was used as the forecast model (Skamarock et al., 2008). The horizontal dimensions represented with a 917 by 550 grids with a resolution of 12 km, and the vertical dimension has 50 layers with a top height of 10 hPa. Referring to the physical solutions selected for strong convection and typhoon in the NCEP, the selected physical schemes include the WRF Single-Moment 6-class (WSM6) microphysical solution, RRTMG long-wave and short-wave radiation schemes, YSU (Yonsei University) boundary layer scheme, and the Tiedtke cumulus parameterization scheme.

3.2 GSI assimilation system

The Gridpoint Statistical Interpolation (GSI) model is a new generation of community global and regional assimilation system that developed based on the NCEP Spectral Statistical Interpolation (SSI) model (Derber and Wu, 1998). It has been widely used in the various meteorological systems, such as the North American Mesoscale Forecast System, the Real-Time Mesoscale Analysis (RTMA) (De Pondeca et al., 2011), Hurricane WRF (HWRF) (Bernardet et al., 2015), and Rapid Refresh System (RR) (Benjamin et al., 2016).

The GSI with a 3DVAR scheme is used to generate initial conditions for the forecast model. The 3DVAR system provides an analysis via the minimization of a prescribed cost function:

$$J(x) = \frac{1}{2}(x-x^b)^T \boldsymbol{B}^{-1}(x-x^b) + \frac{1}{2}[y-H(x)]^T \boldsymbol{R}^{-1}[y-H(x)], \quad (1)$$

where the optimal solution of x, represents a posteriori maximum likelihood estimate of the true atmospheric state given two sources of data: the background x^b and the observations y; $\boldsymbol{B}$ and $\boldsymbol{R}$ are the background and observational error covariance matrices, respectively, which are used to weight the deviation from the analysis to x^b or y; H is the observation operator, transforming the analysis onto observation space. For the 3DVAR experi-

ments, $\boldsymbol{B}$ was estimated using the NMC method (Liu et al., 2015). The observational error covariance matrices $\boldsymbol{R}$ were treated as diagonal matrices with statistically determined variances of the observational data, assuming the observational errors from each source are linearly independent.

3.3 Experiment setup

The assimilation scheme uses the cycle assimilation, and includes three cycles within 12 hours before 72 hours forecast. The background uses the FNL of NCEP GFS. The observational data in this study include conventional observations and satellite observations. The conventional observations mainly include surface synoptic observation (SYNOP), marine buoy data (BUOY), ship data (SHIP), radiosonde observations (RAOB), and the Aircraft/Pilot report data (AIREP/PIREP). The satellite observations are AIRS hyperspectral infrared radiation data.

4 Radiances data assimilation

4.1 Channel selection

There are obvious spatial correlations and spectral similarities among the channels for the hyperspectral infrared observations (Rabier et al., 2002). Therefore, necessary pre-processing for the hyperspectral data was performed before actual application, reducing the channel dimension and removing data redundancy and observation correlation. The AIRS raw data with 2378 channels were processed into a dataset with only 281 channels by the NOAA (National Oceanic and Atmospheric Administration) NESDIS (National Environmental Satellite Data and Information Service), namely the AIRS NRT (Near Real Time) dataset (Fourrié and Thépaut, 2002). However, not all the 281 channels presented in the AIRS NRT channel set are used for assimilation in this study. Channels rejected by NCEP Global Data Assimilation System (GDAS) are also rejected in this study. Excluded channels are those with onboard performance issues, and they are located in the shortwave spectrum and with significant ozone absorption. In addition, AIRS channels that peak around and above 10 hPa level will also be discarded due to the top-level constraint from FNL data. Sensitivity analysis method to determine which channels to be excluded is carried out with the simulated brightness temperature with respect to the change of 1% for temperature (McCarty et al., 2009). Therefore, based on the above methods, a total of 61 channels of data are eventually assimilated into the regional model. Figure 2 shows the weight function of the channel calculated from the standard mid-latitude summer atmospheric profile. The solid lines indicate the selected assimilation channel, while the dashed lines mean the channel discarded by the model top. It can be clearly seen that the excluded channel has a greater contribution at the top levels of the model.

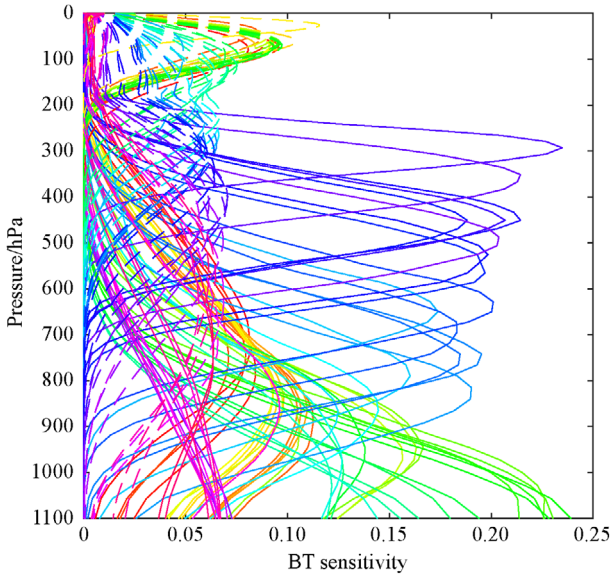

Fig. 2 Weighting functions of 120 AIRS channels assimilated by NCEP GDAS (dotted lines denote the channels discarded by model top; solid lines denote assimilated channels in regional model). Color used to distinguish the various channels. BT sensitivity is calculated with respect to the change of 1% for temperature.

4.2 Quality control

To reduce the spatial correlation of observations, the thin process adopted for AIRS in this study was set 60 km with reference to GDAS (McCarty et al., 2009).

Cloud detection is a key step in the quality control of infrared satellite data. The cloud detection method chosen in this study is based on the scheme proposed by McNally and Watts (2003), which seeks channels that are not affected by the clouds. Figure 3 shows the distribution of O-B (Observation-Background) histograms before and after using this cloud detection method for AIRS channel 253 (13.85 μm). It can be seen that when the cloud detection is not performed (blue line), the O-B histogram clearly has asymmetric structure, and there is a long cold "tail" in the negative value area. Since the O-B distribution (red line) after the cloud detection is clearly symmetrical, the cloud detection in this paper meets the application requirements for data assimilation.

Figure 4 shows the radiance distribution of the AIRS water vapor channel 1627 (7.01 μm) after it finally passed the quality control in GSI. The weight function of the water vapor channel has a relative high peak value and is less affected by the surface, so a large amount of radiation data is assimilated. There is almost no data coverage between Taiwan, China and the Philippines with a large sea area.

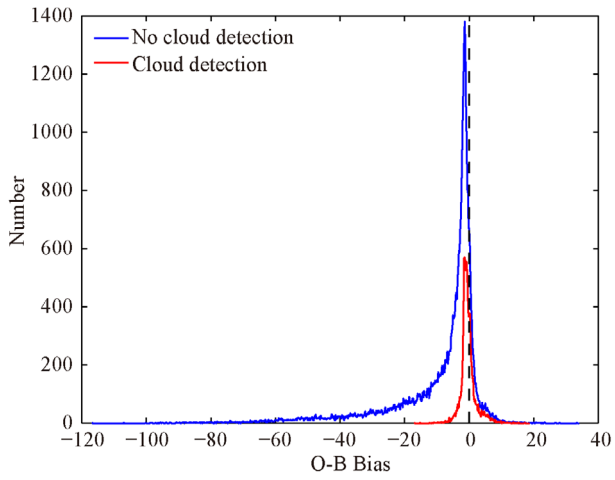

Fig. 3 Histogram of O-B with and without cloud detection for AIRS channel index of 253 (13.85 μm).

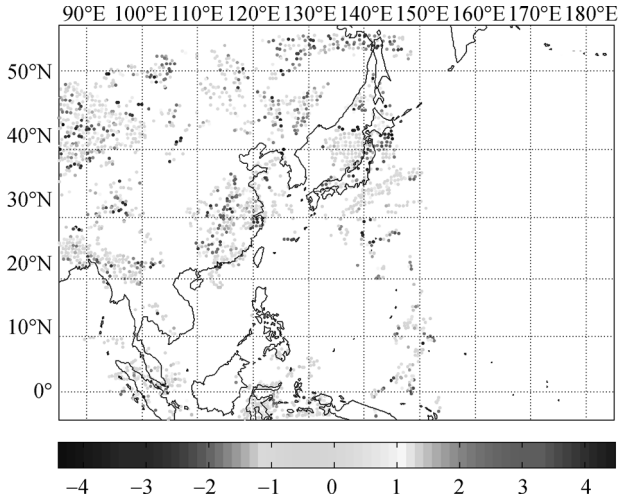

Fig. 4 Innovation (O-B) distributions after the quality control for AIRS channel index of 1627 (7.01 μm).

This is mainly due to the fact that the region was just affected by a typhoon and there were large areas of cloud cover, resulting in almost no available clear-sky infrared radiation data.

4.3 Bias correction

Using bias correction to correct the system bias in the satellite radiance observations is one of the key steps to achieve a successful satellite radiance data assimilation. The bias correction method developed by Derber and Wu (1998) was used in this study. This method includes two aspects. One is angle dependent bias correction, the other is air mass bias correction, also called the variational part of the bias correction. The desired bias correction coefficients are achieved through updating one-month assimilation cycling. The variations of bias correction coefficients in time series were analyzed in detail by Liu et al. (2018). Figure 5 shows the innovation histogram results before and after radiance bias correction for all assimilation channels (except the last channel) in this study. From the histograms, the peak value of the innovation count for most of the channels after correction is close zero, satisfying a necessary condition of Gaussian distribution. Although bias correction is not perfect, it makes sense to identify and remove as many systematic errors as possible. For example, channel 375 (13.17 μm) and water vapor channels 1424 (7.6 μm), 1477 (7.43 μm), and 1500 (7.37 μm) have multiple peaks, which may be due to too limited number of statistical samples in histograms. There are asymmetrical structures for the short-wave CO_2 channels 1865 (4.584 μm), 1868 (4.582 μm), 1873 (4.569 μm), and 1876 (4.563 μm), because these channels belong to the ground channel. As a result, combining the scan angle bias correction and the air mass bias correction methods, through a month of update, the correction coefficients of the assimilated channel can be accurately achieved.

4.4 O-B and O-A analysis

The O-B and O-A (Observation-Analysis) statistics are also very useful information to assess the operation of the assimilation system. Figure 6 shows the comparison of O-B and O-A for all assimilation channels. The bias of 61 channels are significantly reduced after assimilation. For 15 μm CO_2 temperature detection channels, the O-A of almost all channels is very close to zero. The O-A of most of the water vapor channel is also almost close to zero. Short-wave CO_2 channel assimilation after the O-A performance is relatively stable. The O-A of some atmospheric window channels does not reach expectations, which may be caused by the surface emissivity. Overall, the value of O-A is less than O-B after assimilation, indicating that the analysis field after data assimilation is closer to the truth.

4.5 Increment analysis

Analysis of the increments can help to understand the effect of assimilation. This paper analyzes the increment analysis of the temperature in the troposphere (500 hPa) and the water vapor in the low troposphere (850 hPa). In order to compare the influences of AIRS infrared radiation data before and after assimilation, two sets of experiments were set up: 1) Assimilation of conventional observation data only, denoted as Ctrl; 2) Assimilation of both conventional observation data and AIRS infrared radiation data, denoted as Exp. The assimilation cycles at the 12 and 18 UTC were selected, because they can respectively represent the assimilation differences between the limited coverage of AIRS observations. Figure 7 shows the 500 hPa temperature increment at analysis time. From the Ctrl test, Figures 7(b) and 7(d) show that the 1200 UTC has a

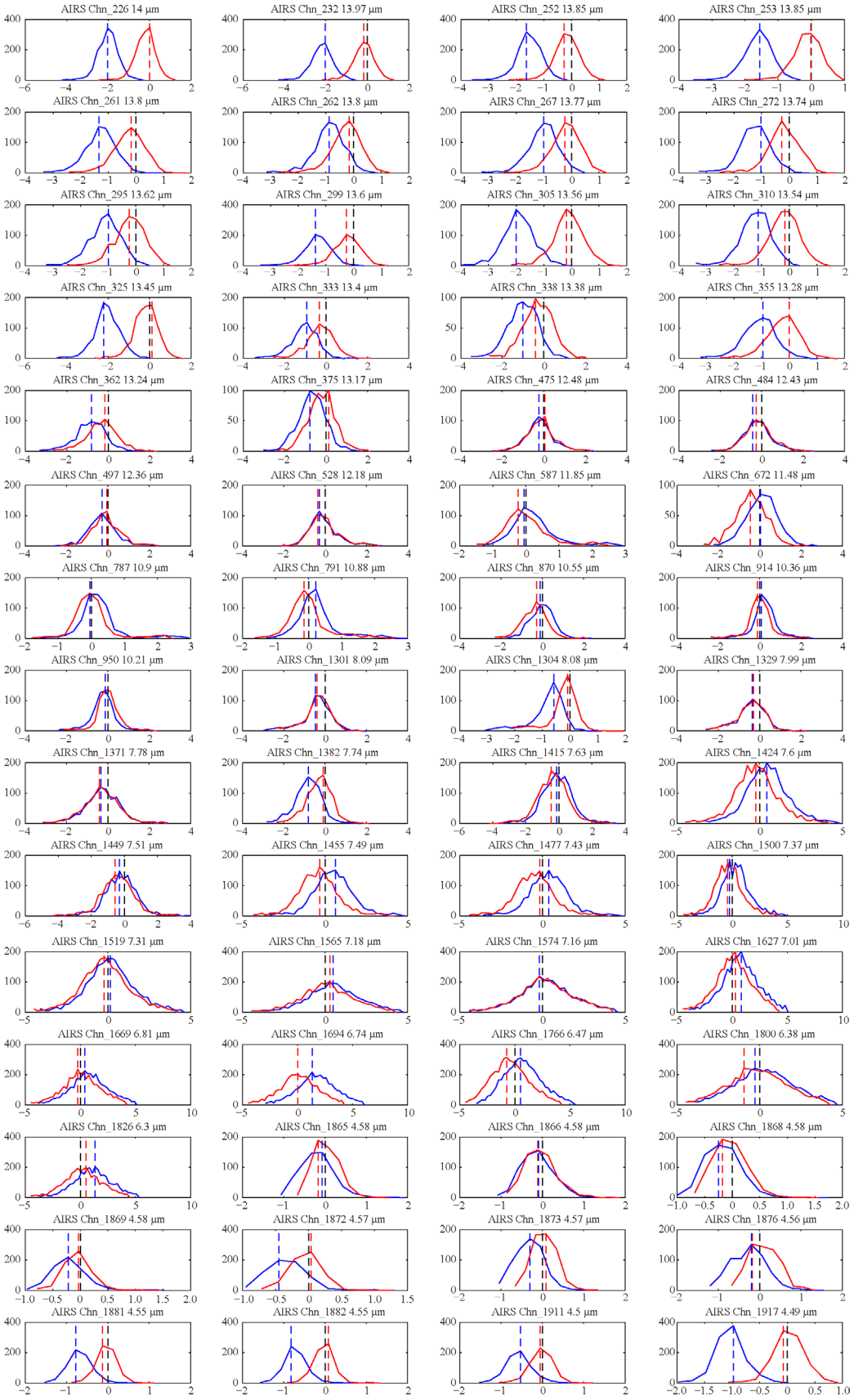

Fig. 5 Histogram of O-F (Observation-First Guess) before (blue) and after (red) bias correction for AIRS assimilated channels at 1800 UTC on July 30, 2012.

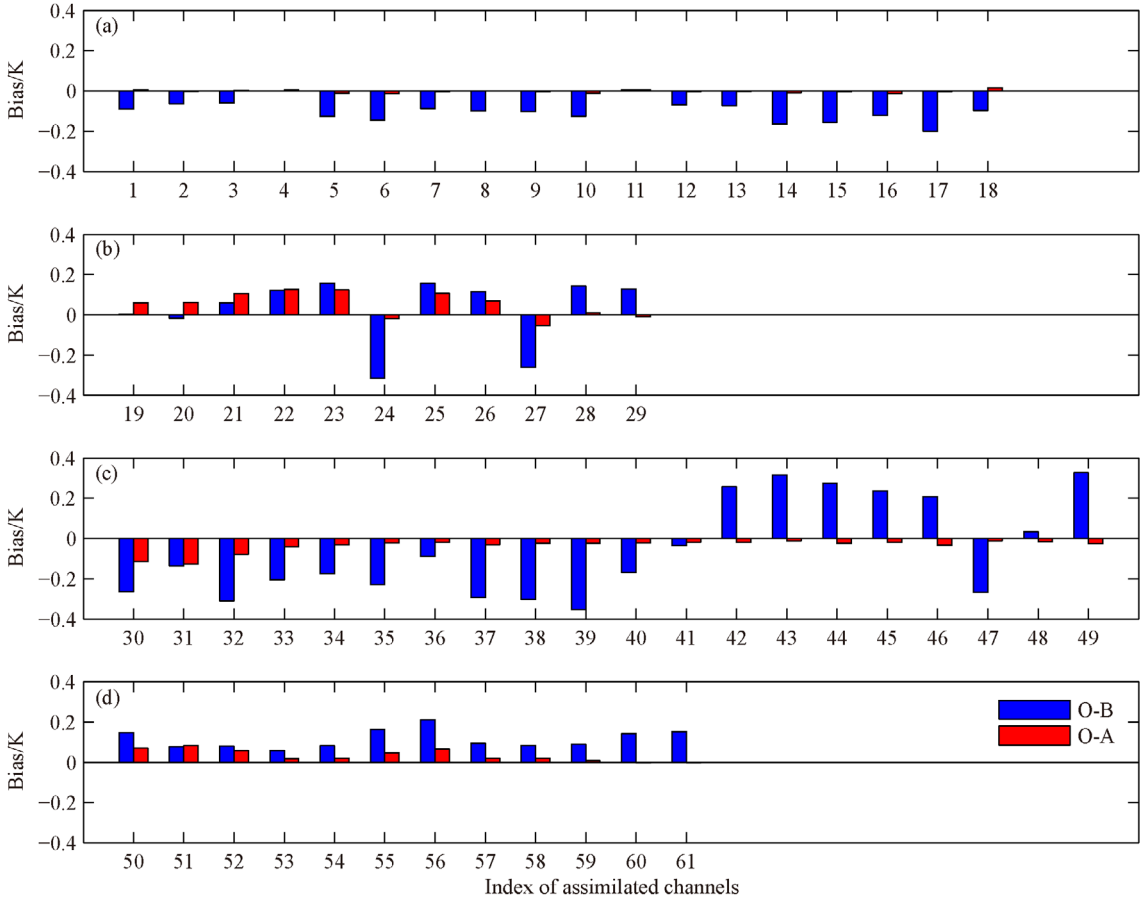

Fig. 6 Bias comparisons of O-B and O-A for all 61 AIRS channels assimilated (the assimilation channel index corresponds to each image in Fig. 5). (a) 15 μm CO_2 channels between 13.2 to 15.4 μm; (b) Window channels between 8.8 to 12.6 μm; (c) H_2O channels between 6.2 to 8.2 μm; (d) Shortwave CO_2 channels between 3.8 to 4.6 μm.

wide range of analysis increment, mainly in the land area, which is related to the distribution of conventional observation data. Compared with the Ctrl, the impact of AIRS observations can be clearly seen. The location of the growth mainly depends on the AIRS data coverage, corresponding to Figs. 1(c) and 1(d). After assimilation of AIRS infrared radiation data in Fig. 7(c), the analysis increment shows a large range of negative values in China, indicating that the temperature was reduced at 500 hPa. Figure 8 shows water vapor analysis increment at the 850 hPa, and the same characteristics can be seen in the temperature analysis.

5 Impact of AIRS data assimilation on typhoon forecast

Based on the previous analysis of the variational assimilation process, this section analyses and compares the effect of cycling assimilation of AIRS radiances on the typhoon forecast. The 72-hour track and intensity forecast for the Ctrl (without assimilating AIRS) and Exp (with assimilating AIRS) were compared with the best available data (Best) from the Joint Typhoon Warning Center (JTWC).

As can be seen from Fig. 9, compared with the best path of JTWC, the absolute error of the 72-hour path forecast for typhoon Saola decreased by nearly 60 km compared with Ctrl, and the average absolute error increased by as much as 15 km after 12-hour spin-up. Due to the roundabout typhoon moving path, the track error does not show the absolute trend of decreasing with the increase of forecast time. In addition to the improvement of the track forecast, the intensity forecast of Exp also had a positive effect. As shown in Fig. 10, both the Ctrl and the Exp are less than Best, which may be determined by the WRF model simulation (0 h) and the large-scale circulation characteristics of the forecast. It also indicates that it is necessary to continuously improve the accuracy of model initial field. The three-day forecast is just a turning point when the typhoon intensity gradually increases and then abruptly weakens. The WRF model forecast can show the entire trend, but there is still a certain amount of deviation, especially after 42 h. However, from the results of control experiments, assimilation of AIRS radiances did increase

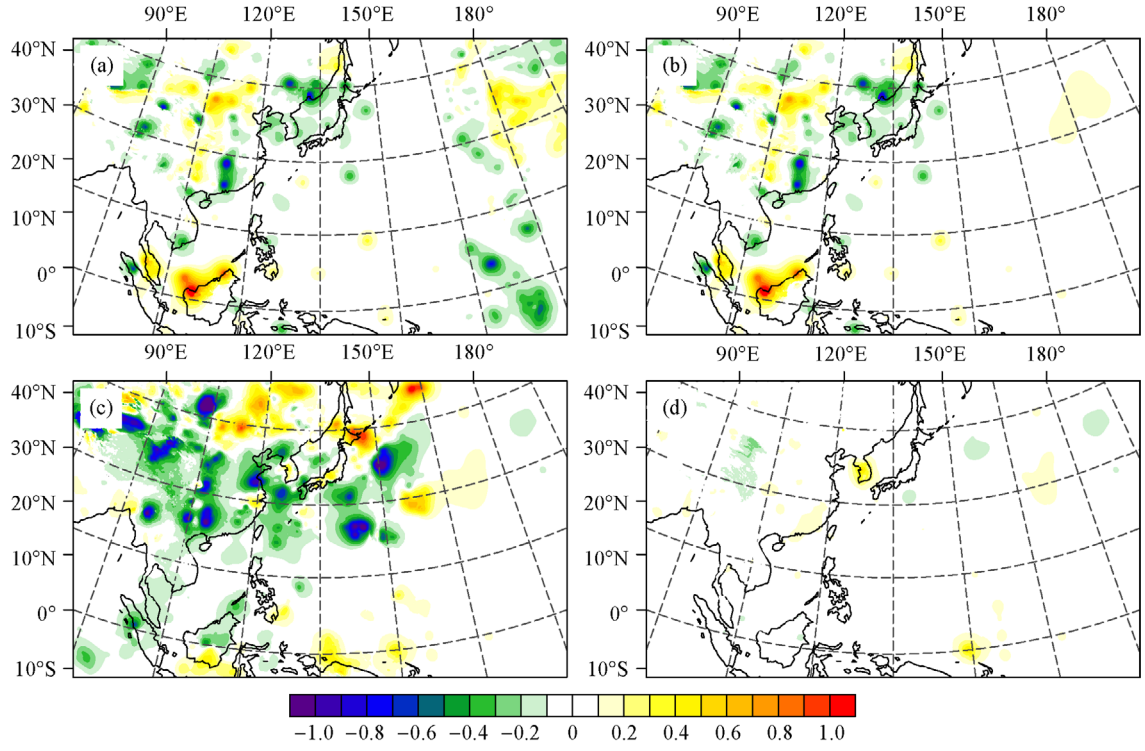

Fig. 7 Comparisons of temperature increment statistics at 500 hPa on July 30, 2012. (a) Exp experiment at 1200 UTC; (b) Ctrl experiment at 1200 UTC; (c) Exp experiment at 1800 UTC; (d) Ctrl experiment at 1800 UTC.

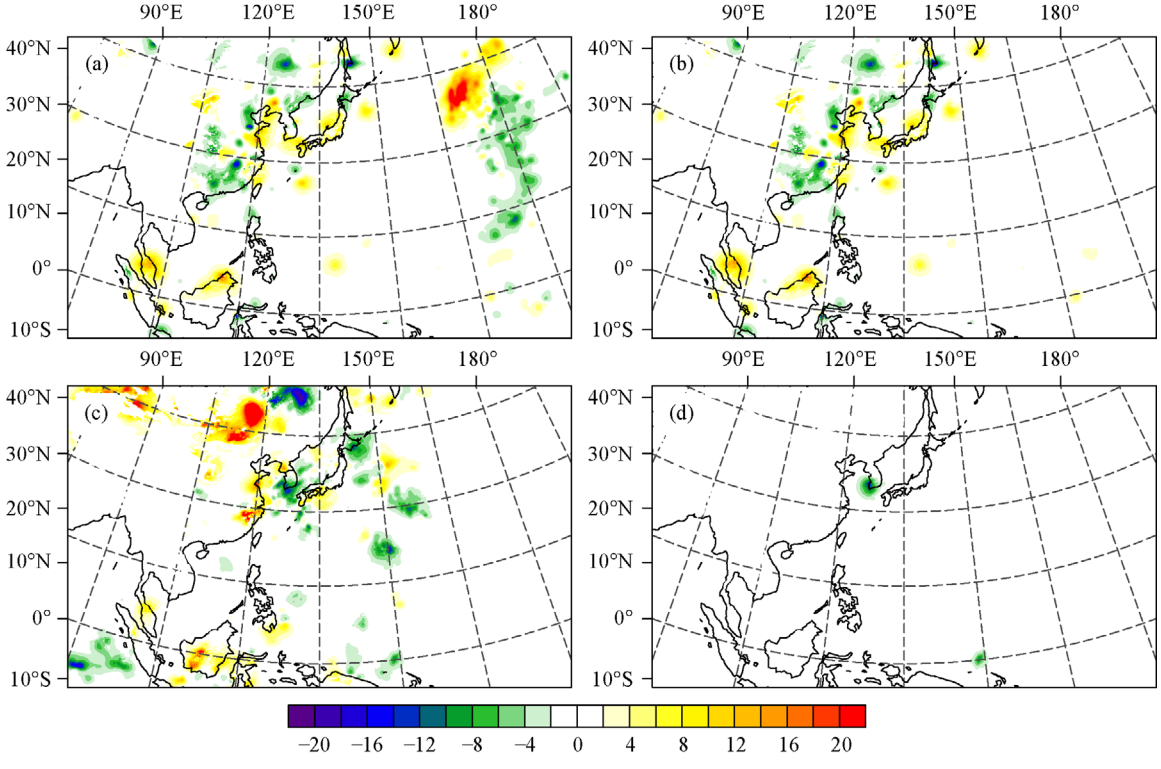

Fig. 8 Comparisons of humidity increment statistics at 850 hPa on July 30, 2012. (a) Exp experiment at 1200 UTC; (b) Ctrl experiment at 1200 UTC; (c) Exp experiment at 1800 UTC; (d) Ctrl experiment at 1800 UTC.

the accuracy of the minimum sea level pressure forecast for the typhoon center.

In order to further analyze the reasons for the improvement of typhoon forecasts after AIRS radiances assimilation, this paper analyze the difference distribution between the Exp analysis field and the Ctrl test analysis field. The distribution at 500 hPa and 850 hPa relative humidity are shown in Fig. 11. The temperature field at 500 hPa of Exp-Ctrl around the typhoon is negative, indicating that the Exp 500 hPa temperature field is lower than Ctrl. Exp-Ctrl's 850 hPa relative humidity distribution indicates that Exp is dryer than Ctrl. Therefore, the intensity of typhoon will be weakened in the drier and low temperature meteorological field, which corresponds to the same phenomenon in Fig. 10 showing higher minimum sea level pressure (weaker intensity) of the Exp and lower minimum sea level pressure of the Ctrl, so the intensity is closer to JTWC.

In order to further strengthen the results, three typhoon cases (Saola, Damrey, and Haikui) were selected between July 27, 2012 and August 10, 2012, and the root mean square error (RMSE) of typhoon track and intensity was calculated for 12 Ctrl and Exp experiments. As shown in Fig. 12, the RMSE of track absolute error is smaller after assimilating AIRS radiances, and the mean track forecast error was decreased by 5.5 km during the entire forecast period. The improvement of typhoon intensity forecast (minimum sea level pressure) is also obvious in Fig. 13, especially after 12 h forecast, and the average improvement is up to 2 hPa.

6 Conclusions

In this study, regional NWP is carried out using GSI coupled with the WRF Model. Hyperspectral infrared data from AIRS are assimilated along with conventional data to improve the typhoon forecast. Assimilation experiments

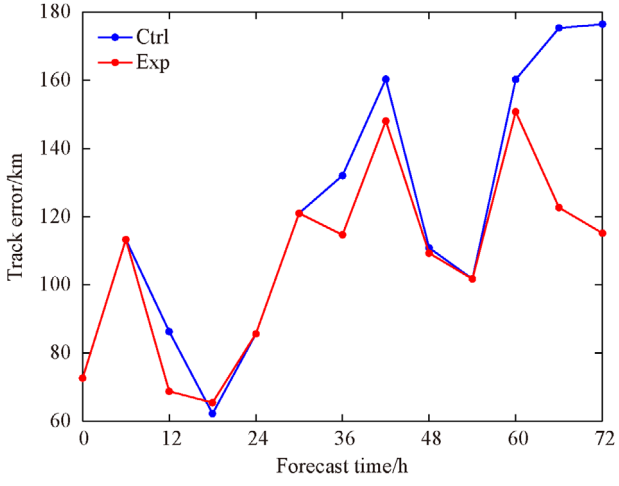

Fig. 9 Comparisons of absolute error of 72 h track forecast for Ctrl and Exp experiment with the best track provided by JTWC (one trial starting from 1800 UTC on July 30, 2012).

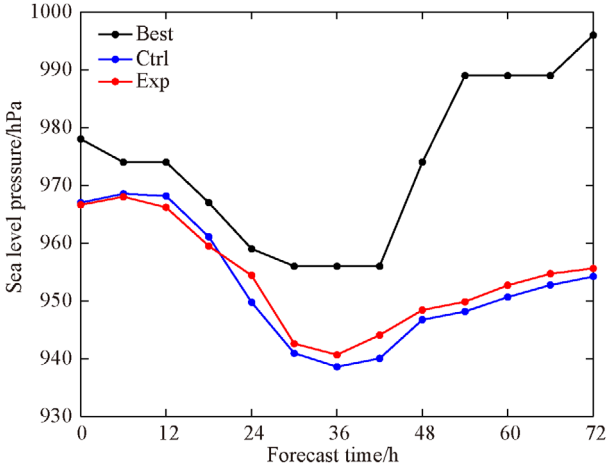

Fig. 10 Comparisons of 72 h minimum sea level pressure forecast for Ctrl and Exp experiment with the intensity provided by JTWC (one trial starting from 1800 UTC on July 30, 2012).

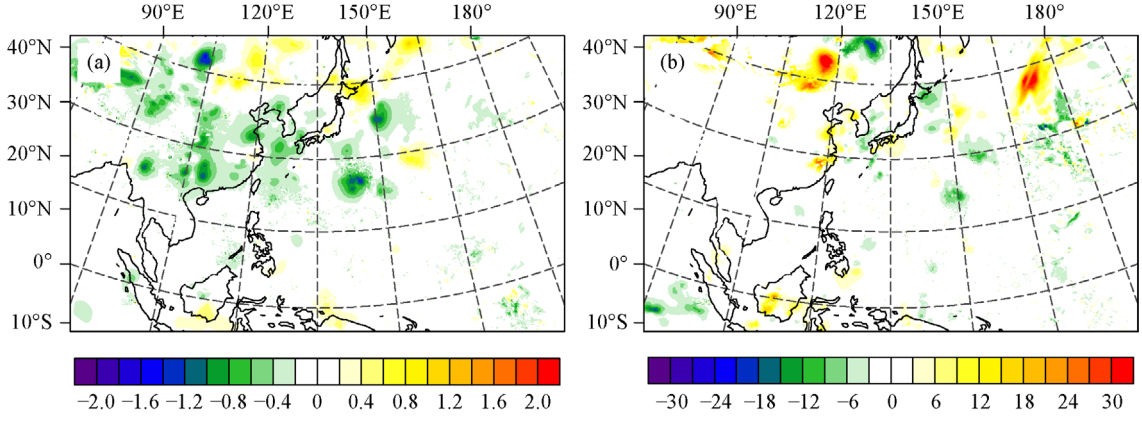

Fig. 11 Exp analysis minus Ctrl analysis. (a) Temperature at 500 hPa; (b) relative humidity at 850 hPa.

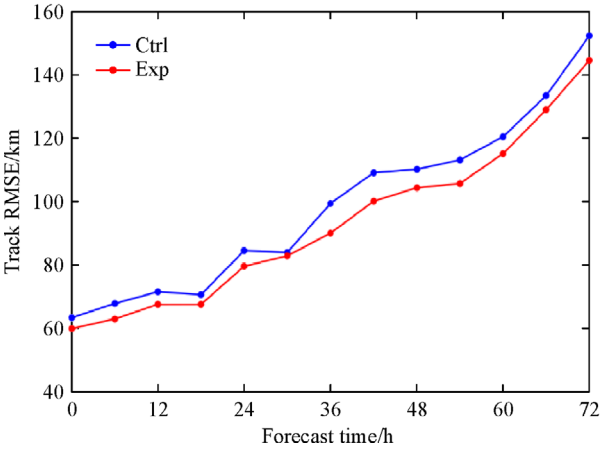

Fig. 12 RMSE comparisons of three typhoon cases' 72 h track forecast with (Exp) and without (Ctrl) AIRS radiances assimilation.

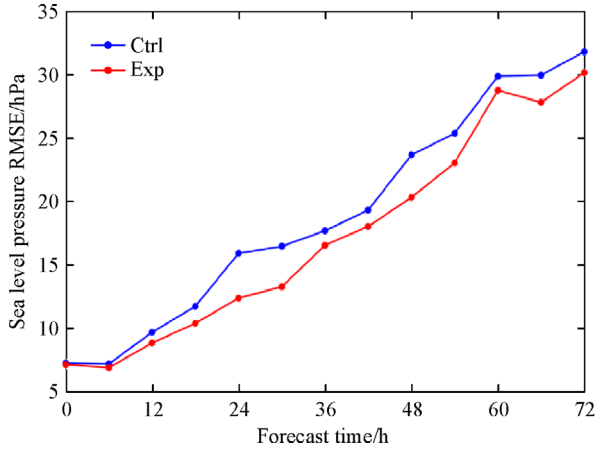

Fig. 13 RMSE comparisons of three typhoon cases' 72 h intensity (minimum sea level pressure) forecast with (Exp) and without (Ctrl) AIRS radiances assimilation.

were carefully designed in various components of the assimilation process, including channel selection, quality control, and bias correction. There were 61 channels eventually selected for inclusion into the assimilation, based on the temperature sensitive method to discard the channel impacted by the model top layer. Combining the scan angle bias correction and the air mass bias correction methods, through a month of update, the correction coefficients of the assimilated channel can be accurately achieved. Both the analysis of O-B and O-A for each channel and the analysis increment show the AIRS radiances assimilation is reasonable in the regional model. As a result, the typhoon track and its intensity are both improved by assimilating the AIRS radiances during the entire forecast period.

In this paper, only three typhoon cases were used to verify the typhoon prediction impact by assimilating AIRS radiances. To further improve the severe weather forecast, we shall further study the meteorological mechanism of more tropical cyclones and assimilate more hyperspectral data, such as the assimilation of IASI (Infrared Atmospheric Sounding Interferometer) and CrIS (Cross-track Infrared Sounder) data.

Acknowledgements This work was supported by the National Natural Science Foundation of China (Grant No. 41601469) and Fundamental Research Funds for the Central Universities in China (East China Normal University). The experiments were run on the Supercomputer located at the Computing Center of East China Normal University.

References

Aumann H H, Chahine M T, Gautier C, Goldberg M D, Kalnay E, Mcmillin L M, Revercomb H, Rosenkranz P W, Smith W L, Staelin D H, Strow L L, Susskind J (2003). AIRS/AMSU/HSB on the aqua mission: design, science objectives, data products, and processing systems. IEEE Trans Geosci Remote Sens, 41(2): 253–264

Bauer P, Thorpe A, Brunet G (2015). The quiet revolution of numerical weather prediction. Nature, 525(7567): 47–55

Benjamin S G, Weygandt S S, Brown J M, Hu M, Alexander C R, Smirnova T G, Olson J B, James E P, Dowell D C, Grell G A, Lin H, Peckham S E, Smith T L, Moninger W R, Kenyon J S, Manikin G S (2016). A North American hourly assimilation and model forecast cycle: the rapid refresh. Mon Weather Rev, 144(4): 1669–1694

Bernardet L, Tallapragada V, Bao S, Trahan S, Kwon Y, Liu Q, Tong M, Biswas M, Brown T, Stark D, Carson L, Yablonsky R, Uhlhorn E, Gopalakrishnan S, Zhang X, Marchok T, Kuo B, Gall R (2015). Community support and transition of research to operations for the hurricane weather research and forecasting model. Bull Am Meteorol Soc, 96(6): 953–960

Carrier M J, Zou X, Lapenta W M (2008). Comparing the vertical structures of weighting functions and adjoint sensitivity of radiance and verifying mesoscale forecasts using AIRS radiance observations. Mon Weather Rev, 136(4): 1327–1348

Carrier M, Zou X, Lapenta W M (2007). Identifying cloud-uncontaminated AIRS spectra from cloudy FOV based on cloud-top pressure and weighting functions. Mon Weather Rev, 135(6): 2278–2294

Chahine M T, Pagano T S, Aumann H H, Atlas R, Barnet C, Blaisdell J, Chen L, Divakarla M, Fetzer E J, Goldberg M, Gautier C, Granger S, Hannon S, Irion F W, Kakar R, Kalnay E, Lambrigtsen B H, Lee S Y, Le MARSHALL J, McMillan W W, McMillin L, Olsen E T, Revercomb H, Rosenkranz P, Smith W L, Staelin D, Strow L L, Susskind J, Tobin D, Wolf W, Zhou L (2006). Improving weather forecasting and providing new data on greenhouse gases. Bull Am Meteorol Soc, 87: 911–926

De Pondeca M S F V, Manikin G S, DiMego G, Benjamin S G, Parrish D F, Purser R J, Wu W S, Horel J D, Myrick D T, Lin Y, Aune R M, Keyser D, Colman B, Mann G, Vavra J (2011). The real-time mesoscale analysis at NOAA's National Centers for Environmental Prediction: current status and development. Weather Forecast, 26(5): 593–612

Derber J C, Wu W S (1998). The use of TOVS cloud-cleared radiances in

the NCEP SSI analysis system. Mon Weather Rev, 126(8): 2287–2299

Eyre J R, Kelly G A, Mcnally A P, Andersson E, Persson A (1993). Assimilation of TOVS radiance information through one-dimensional variational analysis. Q J R Meteorol Soc, 119(514): 1427–1463

Fourrié N, Thépaut J J (2002). Validation of the NESDIS Near Real Time AIRS channel selection. ECMWF Technical Memorandum, 1–14

Goldberg M D, Kilcoyne H, Cikanek H, Mehta A (2013). Joint polar satellite system: the United States next generation civilian polar-orbiting environmental satellite system. J Geophys Res Atmos, 118 (24): 13,463–13,475

Klaes K D, Cohen M, Buhler Y, Schlüssel P, Munro R, Luntama J P, von Engeln A, Clérigh E Ó, Bonekamp H, Ackermann J, Schmetz J (2007). An introduction to the EUMETSAT polar system. Bull Am Meteorol Soc, 88(7): 1085–1096

Le Marshall J, Jung J, Derber J, Chahine M, Treadon R, Lord S J, Goldberg M, Wolf W, Liu H C, Joiner J, Woollen J, Todling R, van Delst P, Tahara Y (2006). Improving global analysis and forecasting with AIRS. Bull Am Meteorol Soc, 87(7): 891–894

Li J, Liu H (2009). Improved hurricane track and intensity forecast using single field-of-view advanced IR sounding measurements. Geophys Res Lett, 36(11): L11813

Lim A H N, Jung J A, Huang H A, Ackerman S A, Otkin J A (2014). Assimilation of clear sky Atmospheric Infrared Sounder radiances in short-term regional forecasts using community models. J Appl Remote Sens, 8(1): 083655

Liu Y A, Huang H L A, Gao W, Lim A H N, Liu C, Shi R (2015). Tuning of background error statistics through sensitivity experiments and its impact on typhoon forecast. J Appl Remote Sens, 9(1): 096051

Liu Y, Huang H A, Lim A H N, Gao W (2018). Adaptive bias correction of advanced infrared sounding radiance assimilation in a regional model and its impact on typhoon forecast. J Appl Remote Sens, 12: 1

McCarty W, Jedlovec G, Miller T L (2009). Impact of the assimilation of Atmospheric Infrared Sounder radiance measurements on short-term weather forecasts. J Geophys Res Atmos, 114: D18122

McNally A P, Watts P D (2003). A cloud detection algorithm for high-spectral-resolution infrared sounders. Q J R Meteorol Soc, 129(595): 3411–3423

McNally P, Watts P D, Smith J, Engelen R, Kelly G, Thépaut J N, Matricardi M (2006). The assimilation of AIRS radiance data at ECMWF. Q J R Meteorol Soc, 132(616): 935–957

Menzel W P, Schmit T J, Zhang P, Li J (2018). Satellite based atmospheric infrared sounder development and applications. Bull Am Meteorol Soc, 99(3): 583–603

Miyoshi T, Kunii M (2012). Using AIRS retrievals in the WRF-LETKF system to improve regional numerical weather prediction. Tellus, Ser A, Dyn Meterol Oceanogr, 64(1): 18408

Pu Z, Zhang L (2010). Validation of atmospheric infrared sounder temperature and moisture profiles over tropical oceans and their impact on numerical simulations of tropical cyclones. J Geophys Res Atmos, 115(D24): 1–13

Rabier F, Fourrie N, Chafai D, Prunet P (2002). Channel selection methods for infrared atmospheric sounding interferometer radiances. Q J R Meteorol Soc, 128(581): 1011–1027

Skamarock W C, Klemp J B, Dudhia J, Gill D O, Barker D M, Duda M G, Huang X Y, Wang W, Powers J G (2008). A Description of the Advanced Research WRF Version 3. NCAR Tech. Notes NCAR/TN-475 + STRT, 1–113

Xu D, Liu Z, Huang X Y, Min J, Wang H (2013). Impact of assimilating IASI radiance observations on forecasts of two tropical cyclones. Meteorol Atmos Phys, 122(1–2): 1–18

Zheng J, Li J J, Schmit T J, Li J J, Liu Z (2015). The impact of AIRS atmospheric temperature and moisture profiles on hurricane forecasts: Ike (2008) and Irene (2011). Adv Atmos Sci, 32(3): 319–335

Zhou Y P, Lau K M, Reale O, Rosenberg R (2010). AIRS impact on precipitation analysis and forecast of tropical cyclones in a global data assimilation and forecast system. Geophys Res Lett, 37: L02806